PCCP

PAPER

View Article Online
View Journal | View Issue

Cite this: *Phys. Chem. Chem. Phys.*, 2016, **18**, 13820

"Pnicogen bonds" or "chalcogen bonds": exploiting the effect of substitution on the formation of P···Se noncovalent bonds†

Rahul Shukla and Deepak Chopra*

Received 13th March 2016,
Accepted 18th April 2016

DOI: 10.1039/c6cp01703g

www.rsc.org/pccp

In this article, we have analyzed the nature and characteristics of P···Se noncovalent interactions by studying the effect of substitution on $XH_2P\cdots SeH_2$, $H_3P\cdots SeHX$ and $XH_2P\cdots SeHX$ (X= −H, −F, $-CH_3$, $-CF_3$, −Cl, −OH, $-OCH_3$, $-NH_2$, $-NHCH_3$, and −CN) as our systems of interest at MP2/aug-cc-pVDZ level of theory. Binding energy calculations depict that binding energy increases in the order $XH_2P\cdots SeH_2 < H_3P\cdots SeHX < XH_2P\cdots SeHX$ with the nature of the substituent having a direct effect on the strength of the interactions. P···Se contacts as short as 2.52 Å were observed and analyzed in our study. The energy values for P···Se contacts were found to exist in the range of −1.20 kcal mol^{-1} to −7.89 kcal mol^{-1}. The topological analysis confirms the presence of P···Se contacts in all the complexes with characteristics similar to hydrogen bonds. NBO analysis helped in categorizing these interactions into pnicogen and chalcogen bonds, depending on the strength of P(lp) to σ*(Se−X) orbitals or Se(lp) to σ*(P−X) orbitals.

Introduction

Studying noncovalent interactions is one of the crucial aspects in supramolecular chemistry.[1–5] Understanding noncovalent interactions has found importance in biological systems.[6–10] While noncovalent interactions such as hydrogen bonds[11–15] and halogen bonds[16–20] are now well established and characterized through experimental and computational methods, the current focus is on unraveling the behavior of other types of noncovalent interactions. Noncovalent interactions such as carbon bonding,[21–23] pnicogen bonding,[24–26] chalcogen bonding,[27–29] and aerogen bonding[30–32] have garnered significant interest in the last few years because of their stabilizing character. Similar to halogen bonding,[33] these noncovalent interactions are characterized by the presence of a positive electrostatic region, labeled as the σ-hole. The σ-hole bond can be defined as the interaction between the covalently bonded atoms of groups IV–VIII and a lone pair present in a Lewis base or an anion.[34] The concept of the σ hole is now well defined in supramolecular chemistry and proven to be a key component in molecular crystals.[35–37]

Pnicogen bonding was first observed in an *ortho*-carbaborane derivative wherein the presence of stabilizing P···P interactions was established through NMR studies.[38,39] P···P interactions were also reported in a series of halogenophosphane functionalized naphthalenes.[40] Pnicogen bonding got prominence when it was demonstrated that P···P bonds can be as strong as H-bonds and can be used as molecular linkers.[24] Another study on pnicogen bonding categorized it as lump–hole interactions.[41] The study on pnicogen bonded complexes involving anions showed the presence of some covalent character in these interactions.[42] The strength of pnicogen bonds involving N, P, and As was also investigated and it was observed to be highly stabilizing.[43] Also in a recent study by Politzer *et al.* it was observed that most of the short contacts involving P and As in crystal structures were indeed σ-hole interactions.[44] The phenomenon of pnicogen bonding was also established from experimental charge density analysis on organic molecules.[45] Several theoretical studies by Professor Steve Scheiner and coworkers have contributed significantly towards the understanding of pnicogen bonding and established it as an important noncovalent interaction.[46–48]

Chalcogens are an important group of elements because of their important role in biological functions.[49–51] Amongst them, selenium is of specific interest because of its role in ligand chemistry[52,53] and organoselenium chemistry.[54,55] Studies involving chalcogen atoms show that these are capable of forming strong noncovalent interactions due to their ability to act as bond acceptors as well as bond donors.[56] Experimental and theoretical charge density analysis has been performed to understand the nature of chalcogen bonding in molecular crystals.[57] Our recent study on chalcogen bonding showed the stabilizing characteristics of Se···O/N contacts.[58] In addition to this, another study, highlighting the role of intermolecular

Crystallography and Crystal Chemistry Laboratory Department of Chemistry, Indian Institute of Science Education and Research Bhopal, Bhopal 462066, Madhya Pradesh, India. E-mail: dchopra@iiserb.ac.in; Fax: +91-075-6692370

† Electronic supplementary information (ESI) available. See DOI: 10.1039/c6cp01703g

interactions involving selenium, was performed on a series of isoselenazolone and monoselenide derivatives.[59] The role of chalcogen bonds involving Se has been further investigated in heterocyclic compounds also.[60] Due to the above mentioned characteristics, it is of extreme importance to understand noncovalent interactions involving selenium.

The aim of this study was to understand the cooperativity between pnicogen bonding and chalcogen bonding by evaluating the nature and strength/characteristics of P···Se contacts in $XH_2P\cdots SeH_2$, $H_3P\cdots SeHX$ and $XH_2P\cdots SeHX$ complexes having an anisotropic electronic environment. The substituents utilized for this study were X = −H, −F, $-CH_3$, $-CF_3$, −Cl, −OH, $-OCH_3$, $-NH_2$, $-NHCH_3$, and −CN. Different substituents are expected to lead to the formation of σ-holes with different strength on phosphorous and selenium atoms and this is expected to alter the nature and strength of P···Se contacts. While a significant number of previous studies have compared the strength and characteristics of pnicogen and chalcogen bonding[61–64] separately, a direct comparison of these interactions where the same atoms are interacting is expected to provide detailed insights into the role of electronic effects in the formation of either pnicogen or chalcogen bonds. Hence, we present a more direct comparison of pnicogen and chalcogen bonds through the formation of P···Se noncovalent interactions.

Computational methods

Second order Møller–Plesset theory (MP2)[65] using the aug-cc-pVDZ level basis set[66] was used to perform all the calculations reported in this study. Several studies on noncovalent interactions have employed this method and reliable results have been obtained.[46,58,67] The results obtained from this method have been found to be comparable to the results obtained by using computationally more expensive CCSD(T) level of theory using a higher basis set.[68–70] Optimization of the starting structure was performed using Gaussian 09[71] package and all optimized structures were verified to be true minima with no imaginary frequencies. All further calculations were performed by utilizing the coordinates of the optimized structures. G09 was further utilized to plot molecular electrostatic potential maps for the atoms participating in noncovalent interactions. Counterpoise-corrected binding energy for all the dimers was evaluated by taking into account the basis set superposition error.[72] Energy decomposition analysis (EDA) was also performed using the LMOEDA module present in GAMESS-US[73,74] to obtain the total binding energies of the complexes partitioned into the corresponding electrostatic, exchange, polarization, repulsion, and dispersion components, respectively. In the EDA methods, the difference between the energy of the supermolecule and the difference between the energy of the monomers constitute the total energy. The electrostatic energy is generally an attractive interaction which originates because of the interaction between the static charge densities of each monomer within the supermolecule. The stabilizing exchange energy arises from the asymmetric nature of the wave function which permits the exchange of electrons between monomers. The evaluation of the repulsion energy requires the energy to be expressed in terms of monomer orbitals that are orthonormal to each other. The polarization contribution is stabilizing and originates because of the relaxation of the supermolecular wave function. The dispersion energy is evaluated by computing the difference in the energy of the system calculated using the MP2 approach and the HF approach. The LMOEDA method has been applied extensively in the analysis of noncovalent interactions.[75–77] The basis set for EDA analysis was obtained from the EMSL basis set library.[78,79] The topological properties such as the electron densities (ρ), Laplacian ($\nabla^2\rho$), local potential energy (V_b), and kinetic potential energy (G_b) at the bond critical point were obtained for all the noncovalent contacts by using AIMALL[80] which is based on the Bader's Theory of Atoms in Molecules.[81] A second-order perturbation energy $E(2)$ calculation was performed using Natural Bond Orbital (NBO) analysis at the DFT level with NBO6[82–84] obtained by integrating it with Gaussian 09. To get a deeper insight into the nature of the interaction, the electron density difference maps were obtained for selected dimers using Multiwfn[85] and plotted using VMD.[86]

Results and discussion

Molecular electrostatic potential maps

Molecular electrostatic potential maps are very helpful in identifying the electron rich and electron deficient regions present in a molecule and have been employed extensively in different studies.[87,88] As established from previous studies, the magnitude of the electropositive region will be maximum on P atoms along the X–P bond.[89] Fig. 1 presents the positive molecular electrostatic potentials plotted for all PH_2X monomers on the total density isosurface with the electrostatic potential ranging from −12 kcal mol^{-1} (red) to 12 kcal mol^{-1} (blue). The maximum magnitude of the positive electrostatic region (σ hole) was observed for X = –F with the magnitude being 31.38 kcal mol^{-1} followed by 30.82 kcal for X = –CN due to the strong electron withdrawing nature of the substituents. The large magnitude of the σ-hole was also observed for X = –Cl and $-CF_3$. In general, the magnitude of the σ hole was clearly dependent on the electronegativity of the atom directly attached to P with the trend being halogens > O > N. The lowest magnitude of the σ hole was observed for X = –H and $-CH_3$ because of their electron donating characteristics. Comparing these magnitudes with those observed for Se in XHSe monomers,[58] the magnitude of the σ hole on P was greater than those observed for Se with the expectation of X = –F and –CN where the magnitude of the σ-hole was slightly less on the P atom as compared to that observed for the corresponding XHSe complex. Fig. S1 (ESI†) shows the magnitudes of the negative electrostatic region on the phosphorous upon substitution and as expected the strength of the negative electrostatic region, in general, depend on the nature of the atom directly attached to phosphorous.

Understanding $XH_2P\cdots SeH_2$ noncovalent bonds

In this section, we have studied the P···Se noncovalent contacts by changing the substitution on XH_2P monomers participating

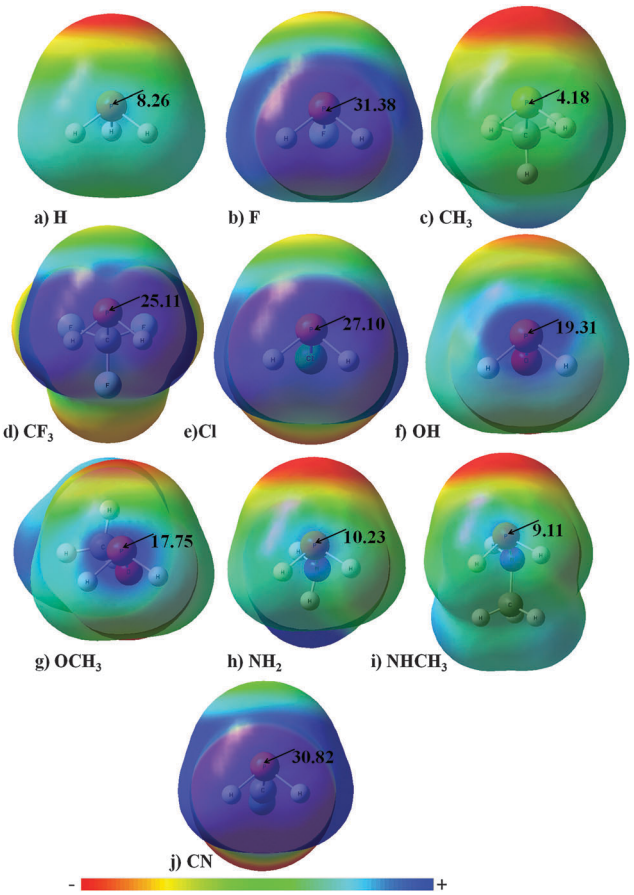

Fig. 1 Electrostatic potential maps for the electrostatic positive regions of monomers (a) H_3P, (b) FH_2P, (c) $(CH_3)H_2P$, (d) $(CF_3)H_2P$, (e) ClH_2P, (f) $(OH)H_2P$, (g) $(OCH_3)H_2P$, (h) $(NH_2)H_2P$, (i) $(NHCH3)H_2P$ and (j) $(CN)H_2P$ on the total density isosurface with potentials ranging from 12 kcal mol^{-1} (red) to 12 kcal mol^{-1} (blue). All energy values are reported in kcal mol-1.

in $XH_2P\cdots SeH_2$ interaction. The aim was to understand the variation in the nature and strength of the P···Se contact on account of the magnitude of the σ-hole on phosphorous. All structures were confirmed to be true minima with no imaginary frequencies. Fig. S2 (ESI†) shows the optimized geometry of all the complexes studied in this section along with the relevant geometrical parameters. The P···Se distance ranged from 3.30 Å (for X = –F) to 3.64 Å (for X = –H). The order of the P···Se distance was observed to be –F < –Cl < $–OCH_3$ < –OH < $–NHCH_3$ < $–NH_2$ < $–CH_3$ ~ –CN < $–CF_3$. All the P···Se interactions were highly directional with the X–P···Se angle being greater than 165° in all cases with the maximum being for X = $–NHCH_3$. Apart from X–P···Se angles, in some cases the H–Se···P angularity were also directional with the magnitude being 161°, 162°, 143°, and 145° for X = –H, $–CH_3$, $–NH_2$, and $–NHCH_3$ substituents, respectively [Fig. S2, ESI†]. Binding energy was evaluated for all the optimized structures and is reported in Table 1. Fig. 2 shows the variation in the binding energy with the changing nature of the substituents. The most stabilized molecular pair was obtained to be X = –F with the magnitude being –3.06 kcal mol^{-1}. The next stabilized molecular pair was for X = –Cl with a binding energy of −2.77 kcal mol^{-1} followed by −2.14 kcal mol^{-1} for X = –CN. Complexes with X = $–OCH_3$, and –OH were having a very similar binding energy of −2.03 kcal mol^{-1} and −2.00 kcal mol^{-1} respectively. Coincidently, the P···Se bond distance was also very close for both the substituents and this may account for a similar binding energy [Table 1]. Similarly, for the nitrogen based substituent *i.e.* X = $–NH_2$ and $–NHCH_3$ the binding energy was similar and here it can also be attributed to a similar P···Se bond distance in these two substituents. The least stabilized pairs were those having substituents X = –H and X = $–CH_3$ due to the absence of electron withdrawing characteristics. The stability of these molecular pairs was complementary to the electropositive region on the phosphorous atom. For comparison, the binding energy of selected complexes was also evaluated at CCSD(T)/aug-cc-pVTZ level of theory and the results were observed to be comparable [Table 1]. Energy decomposition analysis performed on the optimized structures provided deeper insights into the nature of these interactions [Table S1, ESI†]. All the P···Se contacts were dominated by the contribution from the exchange energy followed by the contribution from the electrostatic energy. The contribution of the exchange energy was more than 50% towards stabilization while the contribution of the electrostatic energy was more than 21% in all the cases. The percentage contribution towards stabilization was evaluated by adding the electrostatic, exchange, polarization and dispersion energy terms and dividing the individual terms by the total stabilization energy obtained. This is in accordance with the studies previously done on pnicogen and chalcogen bonds where

Table 1 Geometrical parameters, binding energies, topological parameters, and charge transfer energies obtained for different $XH_2P\cdots SeH_2$ complexes

Criteria	H	CH_3	$NHCH_3$	NH_2	CF_3	OH	OCH_3	CN	Cl	F
P···Se (Å)	3.64	3.60	3.52	3.53	3.62	3.46	3.43	3.60	3.38	3.30
∠X–P···Se (°)	171	169	180	179	165	169	171	165	169	169
∠H–Se···P (°)	161	162	145	143	—	—	—	—	—	—
ΔE (kcal mol^{-1})	−1.20 (−1.25)[a]	−1.38	−1.50	−1.51	−1.76	−2.00	−2.03	−2.14	−2.77	−3.06 (−3.39)[a]
BPL (Å)	3.68	3.63	3.57	3.58	3.65	3.51	3.49	3.62	3.41	3.36
ρ (e $Å^{-3}$)	0.047	0.052	0.060	0.059	0.056	0.070	0.073	0.058	0.084	0.092
$\nabla^2\rho$ (e $Å^{-5}$)	0.431	0.472	0.522	0.516	0.467	0.596	0.615	0.495	0.679	0.747
$\lvert V_b\rvert/G_b$	0.80	0.81	0.840	0.839	0.84	0.87	0.88	0.850	0.91	0.92
$E(2)$ (kcal mol^{-1}) Se(lp) to σ*(P–X)	0.70	0.78	2.25	2.13	2.63	4.51	4.97	3.25	6.64	7.62
$E(2)$ (kcal mol^{-1}) P(lp) to σ*(Se–H)	1.00	1.19	0.97	0.89	—	—	—	—	—	—

[a] Evaluated at the CCSD(T)/aug-cc-pVTZ level.

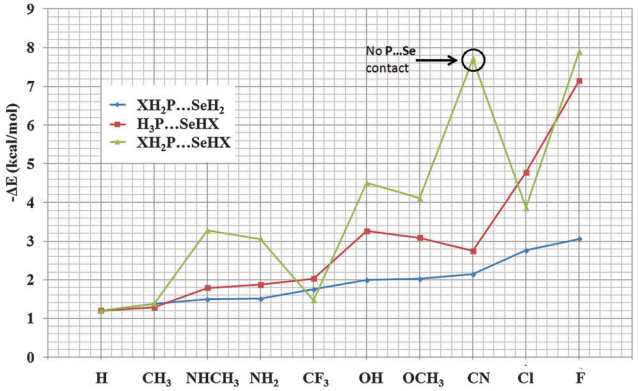

Fig. 2 Variation of binding energy with different substituents for complexes of $XH_2P\cdots SeH_2$, $H_3P\cdots SeHX$ and $XH_2P\cdots SeHX$.

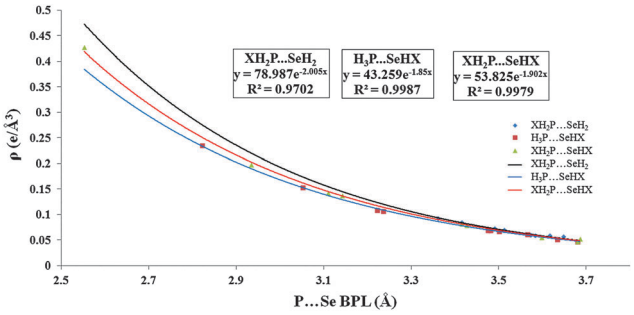

Fig. 3 Plot showing variation of ρ with increasing bond path lengths for different complexes of $XH_2P\cdots SeH_2$, $H_3P\cdots SeHX$ and $XH_2P\cdots SeHX$.

electrostatic and exchange energy terms were the dominant forces.[90,91] The remaining contribution towards stabilization came from dispersion contribution followed by the contribution from polarization energy. The contributions of dispersion energy was greater than polarization energy in all the cases except for X = –F where the contribution of polarization energy was marginally higher. Fig. S6 (ESI†) shows that the magnitude of the electrostatic and exchange energy increases substantially with an increase in the total binding energies of the complexes obtained from decomposition analysis as compared to polarization and dispersion energy where the increase was observed to be of moderate nature. Also, with an increase in the binding energy, there is an increase in the magnitude of each component except for X = –CN where a decrease in the magnitude was observed.

The topological behavior of the P···Se contact was also evaluated and a Bond Critical Point (BCP) was obtained between the P and Se atoms in all the cases [Fig. S13, ESI†]. The value of the Bond Path Length (BPL) ranged from 3.36 Å (for X = –F) to 3.65 Å (for X = –H) and was similar to the corresponding P···Se bond distance [Table 1]. It is important to understand that although the bond distance and the bond path length have similar values, the origins of these values are different.[92] The value of ρ ranged from 0.047 e Å^{-3} (for X = –H) to 0.092 e Å^{-3} (for X = –F), while the value of $\nabla^2\rho$ were all positive with values ranging from 0.431 e Å^{-5} (for X = –H) to 0.747 e Å^{-5} (for X = –F). Fig. 3 shows the plot of ρ against BPL while Fig. S5 (ESI†) shows the variation of $\nabla^2\rho$ with BPL. Both ρ and $\nabla^2\rho$ shows an exponential decay with increasing BPL similar to those observed in the hydrogen bonding.[93] Both ρ and $\nabla^2\rho$ largely followed the trend observed for binding energy except for X = –CN where the binding energy was high but topological values were relatively low. Also, the $|V_b|/G_b$ ratio was observed to be less than one in all the cases, which is similar to hydrogen bonds.[94–96] P···Se contact was observed to follow in general the criteria of Koch and Popelier and was observed to be a closed shell interaction because of the relatively low ρ and positive Laplacian $\nabla^2\rho$.[97]

While it was expected that most of the P···Se noncovalent interactions observed in this section were largely pnicogen bonds as P was having a large magnitude of the positive electrostatic region and Se was acting as an electron donor, there also existed the possibility of formation of the chalcogen bond. In our previous study, it has been shown that selenium[58] has σ hole characteristics even in molecules of SeH_2. To determine this, NBO analysis was also performed to obtain the second order perturbation energy $E(2)$ for all the molecular pairs. Se(lp) to σ*(P–X) was observed for all the molecular pairs with values ranging from 0.70 kcal mol^{-1} (for X = –H) to 7.62 kcal mol^{-1} (for X = –F) [Table 1]. However, in the case of X = –H, CH_3, NH_2, and $NHCH_3$, a significant contribution of the P(lp) to σ*(Se–H) orbital' was also obtained with the values being 1.00, 1.19, 0.89, and 0.97 respectively. Coincidently these molecular pairs exhibited significant values of H–Se···P angles [Fig. S2, ESI†]. This indicates the fact that directionality plays a very crucial role in transitions between orbitals involved in noncovalent bonds. The trend in $E(2)$ for Se(lp) to σ*(P–X) charge transfer was observed not to strictly follow the trend as was observed in binding energy. The reason for this can be attributed to the way these two energies are evaluated. While binding energies consider the interaction between the two molecules taking into account the basis sets of the entire molecule, the $E(2)$ energies only show the contribution coming from a specific set of interacting orbitals. Also, in the case of X = –H and $-CH_3$, the contribution of P(lp) to σ*(Se–H) orbitals was observed to be greater than Se(lp) to σ*(X–P) orbitals indicating that chalcogen bonding character was more prominent in these two cases as compared to pnicogen bonding [Table 1]. This is because of the electron donating characteristics of X = –H and $-CH_3$. The trend in the $E(2)$ was similar to those observed for the energy terms obtained from the total binding energy (from decomposition analysis). Also, comparisons of $E(2)$ with different energy decomposition terms show that the electrostatic and exchange terms increase rapidly with $E(2)$ as compared to dispersion and polarization indicating that exchange and electrostatic terms are major contributors to charge transfer [Fig. S7, ESI†].

Comparing our results with a similar study performed on the P···N pnicogen bond[89] shows that the P···Se distance was larger than the P···N complexes for the corresponding substituents. This larger P···Se distance is accompanied by a decrease in the binding energy as compared to P···N contacts. The magnitude of charge transfer obtained for Se(lp) to σ*(P–X) transitions was also observed to decrease in comparison to N(lp) to σ*(P–X) bonds. The weaker nature of P···Se contacts in comparison to

P···N contacts can be attributed to the nature of N and Se as an electron donor in pnicogen bonds. In a recent study by Scheiner *et al.*, the pnicogen atom (N) was observed to be a better electron donor towards the formation of a pnicogen bond in comparison to the chalcogen atoms.[98,99] Also, the trend in the donor capability of different atoms in the formation of pnicogen bonds was observed to be the reverse of those observed in hydrogen and halogen bonding.[98,99] The anisotropic environment around the Se atom is also important. This is on account of the small σ-hole character on Se. It tends to orient itself towards the lp of P which in turn affects the strength of the P···Se contact.

Understanding $H_3P\cdots SeHX$ noncovalent bonds

In this section, we changed the substitution on XHSe and made to interact with the PH_3 molecule. All the structures obtained after optimization were true minima with no imaginary frequencies. All the optimized structures along with the geometrical parameters and binding energy have been shown in Fig. S3 (ESI†), except for X = –H which is already shown in Fig. S2 (ESI†). The P···Se distance ranges from 2.81 Å for X = –F to 3.60 Å for X = $-CH_3$ with the trend being –F < –Cl < –OH < $-OCH_3$ < $-NH_2$ ~ $-NH_3$ < –CN < $-CF_3$ < $-CH_3$ < –H [Table 2]. Also, the observed P···Se distance, in this case, was shorter than those observed for the corresponding motifs in the previous section [Table 2]. Here also, the X–Se···P angles were very directional with the values ranging from 161° for X = –H to 173° for X = –Cl/–CH_3. In addition to this, the H–P···Se angle was having a directionality of 171° for X = –H and 143° for X = $-NHCH_3$ [Table 2]. All the $XHSe\cdots PH_3$ contacts were more stabilized as the magnitude of the binding energy observed in this section was greater as compared to the binding energies obtained for $XH_2P\cdots SeH_2$ complexes except for X = $-CH_3$ where a decrease in the magnitude of the binding energy was observed [Fig. 2]. The magnitude of the binding energies ranged from −1.20 kcal mol^{-1} for X = –H to −7.15 kcal for X = –F with the trend being –H < $-CH_3$ < $NHCH_3$ < $-NH_2$ < $-CF_3$ < –CN < $-OCH_3$ < –OH < Cl < F [Fig. 2]. There is more than 1.5 fold increase in the stability for X = –Cl while a two-fold increase in the stability for X = –F was observed when compared to the previous section [Tables 1 and 2]. Energy decomposition analysis showed that here also the major contribution towards stability was coming from the exchange energy component with the contribution around 50% in all the cases. The contribution from electrostatic energy ranged from around 20% for X = $-CH_3$ to 30% for X = –CN [Table S2, ESI†]. This is in accordance with the magnitude of the positive electrostatics observed on selenium atoms.[58] Compared to $XH_2P\cdots SeH_2$ complexes, the magnitudes of electrostatic and exchange energy components were much larger in $H_3P\cdots SeHX$ complexes [Table S2, ESI†]. Also, increase in the percentage contribution from electrostatic energy along with a decrease in the percentage contribution from exchange energy as compared to the previous section was observed for all the cases except for X = $-CH_3$ [Table S2, ESI†]. For X = –F, –Cl, –OH, and $-OCH_3$ the percentage contribution from polarization energy was greater than that of dispersion energy while in rest of the case the contribution of the dispersion energy was higher. In addition to electrostatic and exchange energies, for $H_3P\cdots SeHX$ complexes an increase in the contribution from polarization energy was observed with increasing binding energy [Table S2 and Fig. S8, ESI†].

Topological studies on $XHSe\cdots PH_3$ complexes showed the presence of a bond critical point between Se and P atoms in all the cases [Fig. S14, ESI†]. The ρ value ranged from 0.0471 e$Å^{-3}$ for X = –H to 0.235 e $Å^{-3}$ for X = –F [Table 2]. The $\nabla^2\rho$ value ranged from 0.431 e $Å^{-5}$ for X = –H to 1.461 e $Å^{-5}$ for X = –F [Table 2]. Here also, both ρ and $\nabla^2\rho$ followed an exponential trend [Fig. 3 and Fig. S5, ESI†]. The $|V_b|/G_b$ ratio was also observed to be lower than one in all the cases [Table 2]. The magnitudes of ρ and $\nabla^2\rho$ were higher for all the complexes in this section as compared to those observed for corresponding $XH_2P\cdots SeH_2$ complexes. One of the reasons for the high values of topological parameters can be attributed to the short P···Se bond distances observed in the case of selenium substituted complexes. And similar to the previous section, both ρ parameters largely follow the trend observed for the binding energies.

The NBO analysis shows that all interactions have a major contribution from P(lp) to σ*(Se–X) orbitals establishing that all the complexes in this section were having chalcogen bond character. The $E(2)$ values ranged from 0.78 kcal mol^{-1} (for X = –H) to 26.20 kcal mol^{-1} (for X = –F) [Table 2]. Similar to the previous section, here also $E(2)$ does not strictly follow the trend similar to those observed in binding energy. The trend in the charge transfer energy was similar to those observed for the electrostatic and exchange energy terms obtained from energy

Table 2 Geometrical parameters, binding energies, topological parameters, and charge transfer energies obtained for different $H_3P\cdots SeHX$ complexes

Criteria	H	CH_3	$NHCH_3$	NH_2	CF_3	OH	OCH_3	CN	Cl	F
P···Se (Å)	3.64	3.60	3.46	3.46	3.56	3.21	3.23	3.49	3.04	2.81
∠X–Se···P (°)	161	162	170	169	168	172	173	169	173	172
∠H–P···Se (°)	171	171	143	—	—	—	—	—	—	—
ΔE (kcal mol^{-1})	−1.20	−1.28	−1.79	−1.87	−2.03	−3.26	−3.09	−2.75	−4.77	−7.15 (−7.54)[a]
BPL (Å)	3.68	3.63	3.48	3.47	3.56	3.22	3.23	3.50	3.05	2.82
ρ (e $Å^{-3}$)	0.047	0.051	0.070	0.070	0.061	0.109	0.107	0.678	0.154	0.235
$\nabla^2\rho$ (e $Å^{-5}$)	0.431	0.461	0.637	0.650	0.558	0.976	0.952	0.630	1.194	1.461
$\lvert V_b\rvert/G_b$	0.80	0.81	0.83	0.83	0.81	0.90	0.90	0.81	1.00	1.19
$E(2)$ (kcal mol^{-1}) P(lp) to σ*(Se–X)	1.00	0.98	3.34	3.39	2.61	8.08	8.29	3.61	13.44	26.20
$E(2)$ (kcal mol^{-1}) Se(lp) to σ*(P–H)	0.70	1.04	—	—	—	—	—	—	2.39	—

[a] Evaluated at the CCSD(T)/aug-cc-pVTZ level.

decomposition analysis establishing that here also these terms are largely responsible for charge transfer between Se(lp) and σ*(P–X) [Fig. S9, ESI†]. Apart from the electrostatic and the exchange energy, the contribution from polarization energy increased with $E(2)$ while the contribution from dispersion energy does not get affected by increased charge transfer [Fig. S9, ESI†]. In the case of CH_3, however, the contribution from Se(lp) to σ*(P–H) orbital was observed to be 1.05 kcal mol^{-1}. It indicates towards that in the case of $–CH_3$, pnicogen bonding character was strongly prevalent. The presence of significant pnicogen bond character for the X = $–CH_3$ substituted complex is in support of the trend observed in the binding energy and the topological parameters wherein the behavior of X = $–CH_3$ complexes was opposite to rest of the complexes which had predominantly chalcogen bond characteristics.

A comparison of the results obtained on Se···P contact discussed in this section with our previous study on the Se···N chalcogen bond[58] shows that Se···P non-covalent interaction is comparatively weaker. As discussed previously, it is because of the donor capability of the participating atom in the formation of the chalcogen bond. Hence similar to pnicogen bonds,[98,99] chalcogen atoms also follow the trend opposite to those observed for hydrogen and halogen bonds. It is because nitrogen has better donor capability towards the formation of the non-covalent bond due to its highly concentrated electron density. Here also, P has a σ-hole character in PH_3 which can also contribute towards the weak nature of Se···P chalcogen bonds. There was also evidence from the NBO analysis wherein the magnitude of the charge transfer observed in the case of Se···P was lower than the corresponding Se···N interaction.

Understanding XH_2P···SeHX noncovalent bonds

In this section, we have explored the role of combined substitution on both the P as well as the Se atom to study the behavior of the P···Se bond wherein both the atoms can have an impact on the magnitude of the sigma-hole in a significant way. Fig. S4 (ESI†) shows the optimized geometry of all the complexes along with geometrical parameters and binding energy. A possible P···Se contact was observed for all the complexes except for X = –CN where the complex was stabilized by hydrogen bonding in addition to other interactions [Fig. S4 and Table S5, ESI†]. X = –CN will be exempted from further discussion in this section. The P···Se bond distance ranges from 2.52 Å for X = –F to 3.64 Å for X = –H [Table 3]. As compared to XH_2P···SeH_2 and H_3P···SeHX complexes, the P···Se bond distance was observed to be much shorter, especially in the case of halogens. For X = –F, this case is particularly interesting as the bond distance of 2.52 Å was much shorter than the sum of the vdW radius of P and Se.[100] The observed directionality of the X–Se···P angle was observed to be significant in all complexes with values ranging from 157° for X = $–NHCH_3$ to 173° for X = $–OCH_3$. One exemption was X = $–CF_3$ where the significant value of only the X–P···Se angle was observed [Table 3]. In addition to this, complexes with X = –F, CH_3, and Cl showed significant values of the X–P···Se angle in addition to the X–Se···P angle. Apart from P···Se interactions, some complexes showed the possibility of hydrogen bonds also. The complex with X = –OH exhibits the formation of O–H···Se contacts (2.88 Å/123°) in addition to P···Se contacts. N–H···Se interactions were also observed for both X = $–NH_2$ and $–NHCH_3$ substituted complexes [Table S4, ESI†]. These hydrogen bonds will directly affect the binding energy of the complexes involved. The binding energy ranged from −1.20 kcal mol^{-1} (for X = –H) to −7.89 kcal mol^{-1} (for X = –F). Due to the possibility of hydrogen bonding, the binding energy for X = –OH, $–OCH_3$ was observed to be higher than that for X = –Cl. Also an increase in the binding energy of $–NH_2$ and $–NHCH_3$ substituted complexes were observed. The binding energy of XH_2P···SeHX complexes was greater than those observed for the corresponding XH_2P···SeH_2 and H_3P···SeHX complexes except for X = $–CF_3$ where the binding energy was observed to be lowest amongst the three sections while for X = –Cl the binding energy was greater than ClH_2P···SeH_2 but was lower than H_3P···SeHCl [Fig. 2]. Energy decomposition analysis shows that here also the major stabilizing contribution comes from the exchange energy followed by the contribution of the electrostatic energy [Table S3, ESI†]. The effect of the short P···Se contact in the case of X = –F was determined from decomposition analysis as the magnitude of individual energy components was much greater than observed for other complexes. It is noteworthy that the magnitude of the decomposition terms for X = –F was much greater that other complexes [Fig. S10, ESI†]. Also, similarly to those observed for H_3P···SeHX complexes, the contribution from the polarization energy was higher than dispersion energy for X = –F, –Cl, OH, and $–OCH_3$ while in rest

Table 3 Geometrical parameters, binding energies, topological parameters, and charge transfer energies obtained for different XH_2P···SeHX complexes

Criteria	H	CH_3	$NHCH_3$	NH_2	CF_3	OH	OCH_3	CN	Cl	F
P···Se (Å)	3.64	3.55	3.39	3.38	3.67	3.11	3.10	—	2.90	2.52
∠X–Se···P (°)	161	162	157	162	—	167	173	—	166	164
∠X–P···Se (°)	171	171	—	—	159	—	—	—	145	140
ΔE (kcal mol^{-1})	−1.20	−1.38	−3.28	−3.06	−1.47	−4.50	−4.11	−7.71	−3.87	−7.89 (−8.99)[a]
BPL (Å)	3.68	3.60	3.43	3.41	3.68	3.14	3.11	—	2.93	2.55
ρ (e Å^{-3})	0.047	0.055	0.080	0.082	0.0521	0.137	0.143	—	0.197	0.428
$\nabla^2\rho$ (e Å^{-5})	0.431	0.495	0.695	0.711	0.450	1.080	1.156	—	1.311	1.061
$\lvert V_b\rvert/G_b$	0.80	0.82	0.87	0.88	0.83	0.98	0.98	—	1.10	1.64
$E(2)$ (kcal mol^{-1}) P(lp) to σ*(Se–X)	1.00	1.18	3.24	3.75	—	10.02	12.23	—	15.11	50.85
$E(2)$ (kcal mol^{-1}) Se(lp) to σ*(P–X)	0.70	1.18	0.39	0.31	2.23	0.85	1.05	—	8.11	2.327

[a] Evaluated at the CCSD(T)/aug-cc-pVTZ level.

of the case the contribution from the dispersion energy was greater. The high magnitude of binding energy obtained for X = –CN as compared to other complexes [Fig. 2] can be attributed to the presence of multiple interactions in the complex [Fig. S5, ESI†].

The topological analysis confirmed the presence of P···Se BCP for all the complexes except for X = –CN [Fig. S15, ESI†]. The ρ value for the P···Se bond ranged from 0.042 e Å^{-3} for X = –H to 0.427 e Å^{-3} for X = –F. The values of ρ for halogen were observed to be exceptionally high as compared to other complexes in this section. Values of $\nabla^2\rho$ ranged from 0.047 e Å^{-5} to 0.428 e Å^{-5}. Herein also, an exponential trend in ρ and $\nabla^2\rho$ values was observed [Fig. 4 and Fig. S5, ESI†]. In the case of X = –F, the value of $\nabla^2\rho$ was not fitting due to the exceptionally short distance and was excluded from the procedure of fitting to the exponential function. In the case of X = –F and –Cl, the $|V_b|/G_b$ ratio was observed to be greater than one which might be because of the extremely short P···Se distance. In the case of X = –OH, BCP was not observed between selenium and the hydrogen atom even though these fulfill the geometrical criteria for hydrogen bonding.[101] However, BCP was observed between Se and H atoms in the case of X = –NH_2 and –$NHCH_3$. However, the value of topological parameters for H···Se interaction was lower than the values obtained for P···Se contact present in these complexes [Table S4, ESI†].

Significant values of $E(2)$ for P(lp) to σ*(Se–X) was observed for all pairs except for X = –CF_3 where only Se(lp) to σ*(P–X) charge transfer was observed [Table 3]. The absence of chalcogen bond character due to no P(lp) to σ*(Se–X) charge transfer can be the reason for observing a low stabilization energy in the –CF_3 substituted complexes [Fig. 2]. The values of $E(2)$ for P(lp) to σ*(Se–X) ranged from 0.78 kcal mol^{-1} (for X = –H) to 50.85 kcal mol^{-1} (for X = –F). The values of Se(lp) to σ*(P–X) charge transfer ranges from 0.31 kcal mol^{-1} for X = NH_2 to 23.27 kcal mol^{-1} for X = –F. In all cases, the $E(2)$ was substantially greater for P(lp) to σ*(Se–X) charge transfer than the corresponding P(lp) to σ*(Se–X) charge transfer, except for X = –CH_3 where the magnitude of $E(2)$ was found to be equal. In the case of X = –OH, the $E(2)$ value of 1.95 kcal mol^{-1} for Se(lp) to σ*(O–H) was also observed. In addition to this, $E(2)$ values of 1.54 kcal mol^{-1} and 2.19 kcal mol^{-1} were also observed for Se(lp) to σ*(N–H) for X = –NH_2 and –NH_3, respectively [Table S4, ESI†]. Variation of $E(2)$ with the decomposition component for P(lp) to σ*(Se–X) was largely similar to those observed for the P(lp) to σ*(Se–X) [Fig. S11, ESI†]. Since most of the Se to P transitions were having a low $E(2)$ value, there was not much variation observed with respect to the energy decomposition terms. [Fig. S12, ESI†]. The reason for the X = –Cl substituted complex having a lower binding energy can be attributed to the reason that it has a substantial chalcogen, as well as pnicogen bond character as observed from $E(2)$ energies as compared to others, wherein either the pnicogen or chalcogen bonding character was dominant.

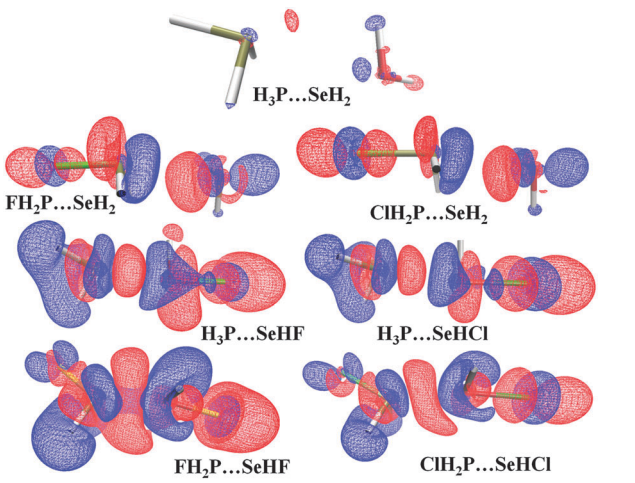

Fig. 4 Electron density difference map for X = –H, –F, and –Cl substituted complexes with a contour value of ±0.0005 a.u. The red and the blue color signify increase and decrease in the electron density upon complex formation, respectively.

Quantitative investigation of the "extremely short" P···Se contact

Although all the complexes we considered for our study were having the P···Se noncovalent bond and was energetically stabilizing, it was of interest to further analyze the extremely short P···Se contacts. These were also observed in the case of F and Cl-substituted complexes due to their strong electron withdrawing nature. This internuclear distance for Se···P was observed to be 2.52 Å, which is 1.13 Å shorter than the sum of the vdW radius[94] of P and Se in the FH_2P···SeHF complex [Table 1]. Similarly for the corresponding X = –Cl substituted complex, the P···Se distance was observed to be 2.90 Å long. Similarly, short values of P···Se was observed for H_3P···SeHX (X = –F and Cl) complexes [Table 2]. As compared to the corresponding XH_2P···SeH_2 complex for halogen substitution, the P···Se distances were relatively high [Table 3]. This shows that the chalcogen bond results in the formation of a shorter bond in comparison to the pnicogen bond and the characteristics of the chalcogen bond increase further when substitution is made simultaneously on P and Se. As discussed earlier, the binding energy in the case of halogen substituted complexes was high as compared to other complexes. As discussed before, the values of the topological parameters were also high for halogen substituted complexes. The results from NBO clearly demonstrate these phenomena. Also, as we have seen that there is some correlation between the bond distances and the stabilizing energy, it is expected that there will be a substantial change in the electronic environment around the participating atom for the short and stronger contacts in comparison to longer contacts. To understand this, we have plotted the energy difference map for all the halogen substituted complexes along with the X = –H substituted complexes for the purpose of comparison [Fig. 4]. The red and blue lobes represent the increase and decrease in the density in the region after complex formation, respectively. One should note that the electron density difference map depends on the model adopted for the calculation and hence doesn't represent a true physical

picture.[102,103] However, it helps in visualizing the effect of substitution in an interaction keeping other factors unchanged. For X = –H, the extent of change in density observed was very less. There is a density depleted region on P accompanied by a region of density accumulation. This region of density accumulation is directed towards the density depleted region on Se. In addition to this, there is also a small density enhanced region on Se, which interacts with the density depleted region on P. It is interesting to note the nature and extent of the change in electron density due to variation in P···Se for X = –F substituted complexes. In $FH_2P\cdots SeH_2$ (P···Se = 3.31 Å), there is a region of enhanced electron density on Se pointing towards a charge depleted region on the P atom leading to the formation of a pnicogen bond. The depleted region on P is caused by the presence of F which experiences an enhancement of electron density after complexation. In the case of $H_3P\cdots SeHF$ (P···Se = 2.81 Å), there exists a density depleted region on P accompanied by the presence of a density enhanced region. This density enhanced region is pointing towards the density depleted region on Se resulting in a strong chalcogen bond. There is also a possibility that the density enhanced region on Se have some access to the density depleted region on P which results in small pnicogen bonding character, as exemplified through NBO analysis. The density difference map for the shortest P···Se contact (2.52 Å) which was observed in $FH_2P\cdots SeHF$ shows that the density depleted region on P and Se are combined into one. Similarly, the charge enhanced region on P and Se is accumulated into one big lobe. Due to this, the charge enhanced region on P has direct access to the charge depleted region on Se resulting in a strong charge transfer from P to Se. Also, the density enhanced region on P has considerable access to the charge depleted region on Se resulting in the presence of small pnicogen bond character. One important observation was the existence of charge enhancement as well as charge depletion occurring on the F atom on both sides due to complex formation. Comparing F substituted complexes with corresponding Cl-substituted complexes, the extent of density enhancement and density depletion is relatively less. Also, the Se···P distances are relatively high for Cl-substituted complexes which also reduces the effective overlap of charge depleted and density enhanced region on both atoms.

A study from the Cambridge Structural Database (CSD):

To compare the results obtained from computational studies, we also screened the Cambridge Structural Database[104] to study the presence of P···Se contacts in molecular crystals. We retrieved a total of 13 crystal structures consisting of sixteen unique P···Se contacts. Table 4 shows the P···Se contacts observed in structures retrieved from the database along with the relevant geometrical parameters. Structures of the retrieved structures have been shown in Table S6 (ESI†). In all cases, the P···Se contact distance was greater than those observed in our model systems. Also, in all cases, the atom participating in P···Se contacts were covalently bonded to P or Se only, except for WUHJUG where the Se was attached to the carbon atom. All the observed structures were also very directional with values ranging from 156° to 178°. In the case of SIDSUT01, both angles *i.e.* Se–P···Se and P–Se···P were high and based on the results we obtained from our theoretical studies it can be expected that it will have significant characteristics of pnicogen as well as chalcogen bonding. In addition to this, the crystal structures wherein the X–P···Se directionality is higher can be attributed to the pnicogen bond while structures, where X–Se···P directionality is higher, can be attributed to the chalcogen bond because as observed from our theoretical study, it is the directionality that plays a very important role in deciding the nature of the interaction.

Table 4 Geometrical parameters for the crystal structures retrieved from the CSD

Refcode	Contact	Distance (Å)	Angle (°)
HEBTIR	Se–P···Se	3.66	156
HEBTIR	Se–Se···P	3.64	162
HEBTIR	P–Se···P	3.62	171
REQQIN	P–P···Se	3.58	173
SIDSUT	Se–P···Se	3.65	169
SIDSUT01	Se–P···Se	3.67	167
	P–Se···P		158
SIDSUT01	P–Se···P	3.59	169
SIDSUT02	Se–P···Se	3.66	169
SIRZUO	P–Se···P	3.65	171
SOVZEI	Se–Se···P	3.65	147
WOQSAW	P–Se···P	3.68	159
WUHJUG	C–Se···P	3.51	178

Conclusions

A systematic study was performed on P···Se noncovalent interactions to understand the effect of substitution. P···Se contact was observed in all the complexes except in the case of the $(CN)H_2$/SeH(CN) complex where P···N pnicogen bonding was observed in addition to other interactions. The most stabilized P···Se contacts were observed in the cases where substitution is made on both phosphorous and selenium simultaneously *i.e.* in $XH_2P\cdots SeHX$ complexes followed by selenium substituted complexes and phosphorous substituted complexes. Apart from this short and directional P···Se contacts were observed in $XH_2P\cdots SeHX$ complexes only with X = –F showing the extremely short P···Se contact of 2.52 Å. Topological studies on P···Se contact showed that properties such as ρ and $\nabla^2\rho$ follow an exponential trend similar to hydrogen bonds. NBO studies were helpful in characterizing the nature of these interactions as pnicogen or chalcogen bonding. Database studies showed that the number of examples forming P···Se contact is scarce, with only one example of P···Se contact in an organic molecule. Also, the distance and directionality observed in crystal structures are significantly different than those observed in our model systems. This indicates that the features of P···Se contacts are still not understood in depth and hence further experimental exploration into this contact is of significance. Further exploration of P···Se contacts is also very important from the biological point of view as both phosphorous and selenium are biologically important atoms.

Acknowledgements

R. S. thanks DST for INSPIRE-PhD Fellowship. We thank Prof. T. N. Guru Row for providing the computational facility in his laboratory. We also thank IISER Bhopal for the research facilities and infrastructure and DST-SERB for research funding.

References

1 M. Raynai, P. Ballester, A. Vidal-Ferran and P. W. N. M. van Leeuwen, *Chem. Soc. Rev.*, 2011, **43**, 1660–1733.
2 H. S. Schneider, T. Schiestel and P. Zimmermann, *J. Am. Chem. Soc.*, 1992, **114**, 7698–7703.
3 A. Tkatchenko, D. Alfé and K. S. Kim, *J. Chem. Theory Comput.*, 2012, **8**, 4317–4322.
4 H. R. Khavasi, A. Ghanbarpour and A. A. Tehrani, *RSC Adv.*, 2016, **6**, 2422–2430.
5 G. R. Desiraju, *Chem. Commun.*, 1997, 1475–1482.
6 N. J. Zondlo, *Nat. Chem. Biol.*, 2010, **6**, 567–568.
7 K. E. Riley and P. Hobza, *Wiley Interdiscip. Rev.: Comput. Mol. Sci.*, 2011, **1**, 3–17.
8 M. Gurusaran, M. Shankar, R. Nagarajan, J. R. Helliwell and K. Sekar, *IUCrJ*, 2014, **1**, 74–81.
9 V. Ball and C. Maechling, *Int. J. Mol. Sci.*, 2009, **10**, 3283–3315.
10 H. Zhu, I. Sommer, T. Lengauer and F. S. Domingues, *PLoS One*, 2008, **3**, e1926.
11 G. R. Desiraju, *Acc. Chem. Res.*, 2002, **35**, 565–573.
12 L. P. Prins, D. N. Reinhoudt and P. Timmerman, *Angew. Chem., Int. Ed.*, 2001, **40**, 2382–2426.
13 D. Dey, T. P. Mohan, B. Vishalakshi and D. Chopra, *Cryst. Growth Des.*, 2014, **14**, 5881–5896.
14 J. U. Bowie, *Curr. Opin. Struct. Biol.*, 2011, **21**, 42–49.
15 G. R. Desiraju and T. Steiner, *The Weak Hydrogen Bond in Structural Chemistry and Biology*, Oxford University Press, Oxford, U.K., 1999.
16 P. Auffinger, F. A. Hays, E. Westhof and P. S. Ho, *Proc. Natl. Acad. Sci. U. S. A.*, 2004, **101**, 16789–16794.
17 R. Wilcken, M. O. Zimmermann, A. Lange, A. C. Joerger and F. M. Boeckler, *J. Med. Chem.*, 2013, **56**, 1363–1388.
18 P. Metrangolo, F. Meyer, T. Pilati, G. Resnati and G. Terraneo, *Angew. Chem., Int. Ed.*, 2008, **47**, 6114–6127.
19 L. C. Gilday, S. W. Robinson, T. A. Barendt, M. J. Langton, B. R. Mullaney and P. D. Beer, *Chem. Rev.*, 2015, **115**, 7118–7195.
20 M. C. Ford and P. S. Ho, *J. Med. Chem.*, 2016, **59**, 1655–1670.
21 D. Mani and E. Arunan, *Phys. Chem. Chem. Phys.*, 2013, **15**, 14377–14383.
22 S. P. Thomas, M. S. Pavan and T. N. Guru Row, *Chem. Commun.*, 2014, **50**, 49–51.
23 E. C. Escudero-Adán, A. Bauzá, A. Frontera and P. Ballester, *ChemPhysChem*, 2015, **16**, 2530–2533.
24 S. Zahn, R. Frank, E. Hey-Hawkins and B. Kirchner, *Chem. – Eur. J.*, 2011, **17**, 6034–6038.
25 L. Guan and Y. Mo, *J. Phys. Chem. A*, 2014, **118**, 8911–8921.
26 J. E. Del Bene, I. Alkorta and J. Elguero, in *Noncovalent Forces: Challenges and Advances in Computational Chemistry and Physics*, ed. S. Scheiner, Springer: New York, 2015, vol. 19, pp. 191–263.
27 W. Wang and B. Ji, Yu. Zhang, *J. Phys. Chem. A*, 2009, **113**, 8132–8135.
28 S. Tsuzuki and N. Sato, *J. Phys. Chem. B*, 2013, **117**, 6849–6855.
29 G. E. Garrett, G. L. Gibson, R. N. Straus, D. S. Seferos and M. S. Taylor, *J. Am. Chem. Soc.*, 2015, **137**, 4126–4133.
30 A. Bauzá and A. Frontera, *Angew. Chem., Int. Ed.*, 2015, **54**, 7340–7343.
31 A. Bauzá and A. Frontera, *Phys. Chem. Chem. Phys.*, 2015, **17**, 24748–24753.
32 A. Bauzá and A. Frontera, *ChemPhysChem*, 2015, **16**, 3625–3630.
33 T. Clark, M. Hennemann, J. S. Murray and P. Politzer, *J. Mol. Model.*, 2007, **13**, 291–296.
34 P. Politzer, J. S. Murray and T. Clark, *Phys. Chem. Chem. Phys.*, 2013, **15**, 11178–11189.
35 M. H. Kolář, P. Carloni and P. Hobza, *Phys. Chem. Chem. Phys.*, 2014, **16**, 19111–19114.
36 P. Politzer, J. S. Murray and P. Lane, *Int. J. Quantum Chem.*, 2007, **107**, 3046–3052.
37 K. J. Donald and M. Tawfik, *J. Phys. Chem. A*, 2013, **117**, 14176–14183.
38 W. E. Hill and L. M. Silva-Trivino, *Inorg. Chem.*, 1978, **17**, 2495–2498.
39 W. E. Hill and L. M. Silva-Trivino, *Inorg. Chem.*, 1979, **18**, 361–364.
40 P. Kilian, A. M. Z. Slawin and J. D. Woollins, *Chem. – Eur. J.*, 2003, **9**, 215–222.
41 K. Eskandri and N. Mahmoodabadi, *J. Phys. Chem. A*, 2013, **117**, 13018–13024.
42 J. E. Del Bene, I. Alkorta and J. Elguero, *J. Phys. Chem. A*, 2014, **118**, 3386–3392.
43 D. Setiawan, E. Kraka and D. Cremer, *J. Phys. Chem. A*, 2015, **119**, 1642–1656.
44 P. Politzer, J. S. Murray, G. V. Janjić and S. D. Zarić, *Crystals*, 2014, **4**, 12–31.
45 S. Sarkar, M. S. Pavan and T. N. Guru Row, *Phys. Chem. Chem. Phys.*, 2015, **17**, 2330–2334.
46 S. Scheiner, *Acc. Chem. Res.*, 2013, **46**, 280–288.
47 S. Scheiner, *Int. J. Quantum Chem.*, 2013, **113**, 1609–1620.
48 U. Adhikary and S. Scheiner, *J. Chem. Phys.*, 2011, **135**, 184306.
49 P. Metrangolo and G. Resnati, *Nat. Chem.*, 2012, **4**, 437–438.
50 L. Engman, D. Stern, H. Frisell, K. Vessman, M. Berglund, B. Ek and C. G. Andersson, *Bioorg. Med. Chem.*, 1995, **3**, 1255–1262.
51 S. T. Manjare, Y. Kim and D. G. Churchill, *Acc. Chem. Res.*, 2014, **47**, 2985–2998.
52 D. Das, P. Singh, M. Singh and A. K. Singh, *Dalton Trans.*, 2010, **39**, 10876–10882.
53 Y. Nishibayashi and S. Uemura, *Top. Curr. Chem.*, 2000, **208**, 235–255.
54 S. J. Balkrishna, S. Kumar, G. K. Azad, B. S. Bhakuni, P. Panini, N. Ahalawat, R. S. Tomar, M. R. Detty and S. Kumar, *Org. Biomol. Chem.*, 2014, **12**, 1215–1219.

55 S. J. Balkrishna, B. S. Bhakuni and S. Kumar, *Tetrahedron*, 2011, **67**, 9565–9575.
56 P. Politzer, J. S. Murray and M. C. Concha, *J. Mol. Model.*, 2008, **14**, 659–665.
57 S. P. Thomas, K. Satheeshkumar, G. Mugesh and T. N. Guru Row, *Chem. – Eur. J.*, 2015, **21**, 6793–6800.
58 R. Shukla and D. Chopra, *J. Phys. Chem. B*, 2015, **119**, 14857–14870.
59 S. J. Balkrishna, R. Shukla, J. P. Jasinski and S. Kumar, *Proc. Natl. Acad. Sci., India, Sect. A*, 2014, **84**, 165–177.
60 J. S. Murray, P. Lane and P. Politzer, *Int. J. Quantum Chem.*, 2008, **108**, 2770–2781.
61 S. Scheiner, *Int. J. Quantum Chem.*, 2013, **113**, 1609–1620.
62 S. Scheiner, *CrystEngComm*, 2013, **15**, 3119–3124.
63 A. Bauzá, D. Quiñonero, P. M. Deyá and A. Frontera, *CrystEngComm*, 2013, **15**, 3137–3144.
64 A. Bauzá, I. Alkorta, A. Frontera and J. Elguero, *J. Chem. Theory Comput.*, 2013, **9**, 5201–5210.
65 M. Head-Gordon, J. A. Pople and M. J. Frisch, *Chem. Phys. Lett.*, 1988, **153**, 503–506.
66 R. A. Kendall, T. H. Dunning Jr. and R. J. Harrison, *J. Chem. Phys.*, 1992, **96**, 6796–6806.
67 U. Adhikari and S. Scheiner, *Chem. Phys. Lett.*, 2012, **532**, 31–35.
68 D. Hauchecorne and W. A. Herrebout, *J. Phys. Chem. A*, 2013, **117**, 11548–11557.
69 J. Wu, *Int. J. Quantum Chem.*, 2011, **111**, 4247–4254.
70 U. Adhikari and S. Scheiner, *J. Phys. Chem. A*, 2014, **118**, 3183–3192.
71 M. J. Frisch, G. W. Trucks, H. B. Schlegel, G. E. Scuseria, M. A. Robb, J. R. Cheeseman, G. Scalmani, V. Barone, B. Mennucci, G. A. Petersson, H. Nakatsuji, M. Caricato, X. Li, H. P. Hratchian, A. F. Izmaylov, J. Bloino, G. Zheng, J. L. Sonnenberg, M. Hada, M. Ehara, K. Toyota, R. Fukuda, J. Hasegawa, M. Ishida, T. Nakajima, Y. Honda, O. Kitao, H. Nakai, T. Vreven, J. A. Montgomery, Jr., J. E. Peralta, F. Ogliaro, M. Bearpark, J. J. Heyd, E. Brothers, K. N. Kudin, V. N. Staroverov, R. Kobayashi, J. Normand, K. Raghavachari, A. Rendell, J. C. Burant, S. S. Iyengar, J. Tomasi, M. Cossi, N. Rega, J. M. Millam, M. Klene, J. E. Knox, J. B. Cross, V. Bakken, C. Adamo, J. Jaramillo, R. Gomperts, R. E. Stratmann, O. Yazyev, A. J. Austin, R. Cammi, C. Pomelli, J. W. Ochterski, R. L. Martin, K. Morokuma, V. G. Zakrzewski, G. A. Voth, P. Salvador, J. J. Dannenberg, S. Dapprich, A. D. Daniels, Ö. Farkas, J. B. Foresman, J. V. Ortiz, J. Cioslowski and D. J. Fox, *Gaussian 09, Revision E.01*, Gaussian, Inc.,Wallingford CT, 2009.
72 S. F. Boys and F. Bernardi, *Mol. Phys.*, 1970, **19**, 553–566.
73 M. W. Schmidt, K. K. Baldridge, J. A. Boatz, S. T. Elbert, M. S. Gordon, J. H. Jensen, S. Koseki, N. Matsunaga, K. A. Nguyen, S. Su, T. L. Windus, M. Dupuis and J. A. Montgomery, *J. Comput. Chem.*, 1993, **14**, 1347–1363.
74 M. S. Gordon and M. W. Schmidt, Advances in electronic structure theory: GAMESS a decade later, in *Theory and Applications of Computational Chemistry: the First Forty Years*, ed. C. E. Dykstra, G. Frenking, K. S. Kim and G. E. Scuseria, Elsevier, Amsterdam, 2005, pp. 1167–1189.
75 P. Su, Z. Jiang, Z. Chen and W. Wu, *J. Phys. Chem. A*, 2014, **118**, 2531–2542.
76 F. Yu, *Int. J. Quantum Chem.*, 2013, **113**, 2355–2360.
77 Y. Chen and H. Li, *J. Phys. Chem. A*, 2010, **114**, 11719–11724.
78 D. Feller, *J. Comput. Chem.*, 1996, **17**, 1571–1586.
79 K. L. Schuchardt, B. T. Didier, T. Elsethagen, L. Sun, V. Gurumoorthi, J. Chase, J. Li and T. L. Windus, *J. Chem. Inf. Model.*, 2007, **47**, 1045–1052.
80 T. A. Keith, *TK Gristmill Software*, Overland Park KS, USA, 2013.
81 R. F. W. Bader, *Atoms in Molecules: A Quantum Theory*, Oxford University Press, 1990.
82 A. E. Reed, L. A. Curtiss and F. Weinhold, *Chem. Rev.*, 1988, **88**, 899–926.
83 A. E. Reed, F. Weinhold, L. A. Curtiss and D. J. Pochatko, *J. Chem. Phys.*, 1986, **84**, 5687–5705.
84 E. D. Glendening, J. K. Badenhoop, A. E. Reed, J. E. Carpenter, J. A. Bohmann, C. M. Morales, C. R. Landis and F. Weinhold, *NBO 6.0*, Theoretical Chemistry Institute, University of Wisconsin, Madison, WI, 2013.
85 T. Lu and F. J. Chen, *Comput. Chem.*, 2012, **33**, 580–592.
86 W. Humphrey, A. Dalke and K. Schulten, *J. Mol. Graphics*, 1996, **14**, 33–38.
87 J. D. Mottishaw, A. R. Erck, J. H. Kramer, H. Sun and M. Koppang, *J. Chem. Educ.*, 2015, **92**, 1846–1852.
88 I. Khan, P. Panini, S. Ud-Din Khan, U. A. Rana, H. Andleeb, D. Chopra, S. Hameed and J. Simpson, *Cryst. Growth Des.*, 2016, **16**, 1371–1386.
89 S. Scheiner, *J. Phys. Chem. A*, 2011, **115**, 11202–11209.
90 U. Adhikari and S. Scheiner, *Chem. Phys. Lett.*, 2012, **532**, 31–35.
91 H. Zhuo, Q. Li, W. Li and J. Cheng, *New J. Chem.*, 2015, **39**, 2067–2074.
92 R. F. W. Bader, *J. Phys. Chem. A*, 2009, **113**, 10391–10396.
93 U. Koch and P. L. A. Popelier, *J. Phys. Chem.*, 1995, **99**, 9747–9754.
94 I. Mata, I. Alkorta, E. Molins and E. Espinosa, *Chem. – Eur. J.*, 2010, **16**, 2442–2452.
95 E. Espinosa, I. Alkorta, J. Elguero and E. Molins, *J. Chem. Phys.*, 2002, **117**, 5529–5542.
96 E. Espinosa, I. Alkorta, I. Rozas, J. Elguero and E. Molins, *Chem. Phys. Lett.*, 2001, **336**, 457–461.
97 P. L. A. Popelier, *J. Phys. Chem. A*, 1998, **102**, 1873–1878.
98 S. Scheiner and U. Adhikary, *J. Phys. Chem. A*, 2011, **115**, 11101–11110.
99 S. Scheiner, *J. Chem. Phys.*, 2011, **134**, 164313.
100 A. Bondi, *J. Phys. Chem.*, 1964, **68**, 441–451.
101 E. Arunan, G. R. Desiraju, R. A. Klein, J. Sadlej, S. Scheiner, I. Alkorta, D. C. Clary, R. H. Crabtree, J. J. Dannenberg, P. Hobza, H. G. Kjaergaard, A. C. Legon, B. Mennucci and D. J. Nesbitt, *Pure Appl. Chem.*, 2011, **83**, 1637–1641.
102 P. Politzer, J. S. Murray and T. Clark, *J. Mol. Model.*, 2015, **21**, 52.
103 T. Clark, *Wiley Interdiscip. Rev.: Comput. Mol. Sci.*, 2015, **5**, 169–177.
104 F. H. Allen, *Acta Crystallogr.*, 2002, **B58**, 380–388.